CCFE
CULHAM CENTRE FOR FUSION ENERGY

UK Atomic Energy Authority

UKAEA-CCFE-PR(23)05

S. Von Tiedemann, D Collins, M. Gilbert, I. Kodeli

Nuclear Data Uncertainty Propagation and Implications for Radioactive Waste Management of Fusion Steels

Nuclear Data Uncertainty Propagation and Implications for Radioactive Waste Management of Fusion Steels

S. Von Tiedemann, D Collins, M. Gilbert, I. Kodeli

This is a preprint of a paper submitted for publication in
Fusion Engineering and Design

Highlights

Nuclear Data Uncertainty Propagation and Implications for Radioactive Waste Management of Fusion Steels

Sophia O. von Tiedemann, David M. Collins, Mark R. Gilbert, Ivan A. Kodeli

- Nuclear fusion activation calculations were performed using FISPACT-II
- Sensitivity and uncertainty analysis carried out with XSUN-2022 code package
- Large parts of reactor exceeded UK low-level activity limits for centuries
- Uncertainties in nuclide production larger in rear of blanket than in first wall
- Nuclear data uncertainties affected decay time by several years

Nuclear Data Uncertainty Propagation and Implications for Radioactive Waste Management of Fusion Steels

Sophia O. von Tiedemann[a,*], David M. Collins[a], Mark R. Gilbert[b], Ivan A. Kodeli[b]

[a] *University of Birmingham, School of Metallurgy and Materials, Edgbaston, Birmingham, B15 2TT, United Kingdom*

[b] *United Kingdom Atomic Energy Authority, Culham Centre for Fusion Energy, Culham Science Centre, Abingdon, OX14 3DB, United Kingdom*

Abstract

Predictions of material activity in commercial fusion conditions predominantly rely on computational methods, due to a lack of data on long-term effects of high-energy neutron irradiation on structural steels. Consequently, this could result in a bias due to uncertainties in nuclear data used. This work focused on modelling neutron activation of four structural steels in a fusion reactor environment after 20 years of operation. Eurofer, F82H and G91, were assessed as candidate in-vessel materials, whereas SS316L(N)-IG was solely modelled in the vacuum vessel. Activation calculations were performed using the inventory code FISPACT-II using inputs from Monte-Carlo transport simulations performed with OpenMC. The study employed a one-dimensional reactor model with a Helium-Cooled Pebble Bed (HCPB) tritium-breeding blanket design. With the XSUN-2022 code package, a nuclear data sensitivity and uncertainty analysis on production cross-sections of relevant radionuclides was carried out. Eurofer and F82H steels exhibited significantly higher resistance to neutron activation than G91 and SS316L(N)-IG. At 100 years after shutdown, none of the steels reached UK low-level waste (LLW) activity levels in the first wall. In the rear of the back-support structure (BSS) of the reactor blanket, all assessed steels reached LLW levels within approximately 30 to 45 years of reactor shutdown. It was found that the vacuum vessel (SS316L(N)-IG) would not be classifiable as LLW for several centuries. Dominant radio-nuclides for each material were identified with FISPACT-II to carry out the uncertainty analyses. The calculated uncertainties were too small to affect the waste disposal options for the first wall within 100 years, but the time-to-reach LLW for BSS and vacuum vessel steel could be uncertain by up to approximately 3 and 6 years, respectively.

Keywords: Nuclear data, Radioactive waste, Fusion steels, Uncertainty propagation, Sensitivity studies

*Corresponding author

Email address: s.o.vontiedemann@bham.ac.uk (Sophia O. von Tiedemann)

1. Introduction

Amid the growing global energy demand and pressure to move away from fossil fuels, nuclear fusion is becoming an increasingly attractive energy source. Where power from nuclear fission produces high-level radioactive waste (HLW), nuclear fusion is anticipated to produce only intermediate- and low-level waste (ILW and LLW), making it more sustainable and favourable over traditional fission power plants. Although the fusion reaction of tritium and deuterium does not directly create any radioactive products, it results in the emission of high-energy (14 MeV) neutrons. Upon interaction with surrounding materials in the reactor wall, these neutrons can lead to activation and the production of significant volumes of radioactive waste (RW) through transmutation, as well as extensive damage in the material structure through atomic displacement [1]. Structural and other in-vessel materials are anticipated to be the major source of RW from fusion.

Due to a lack of existing experimental data on the long-term effects of material exposure to such high-energy neutron irradiation, predictions of resulting RW activities rely heavily on computational models and approaches. Such methods, however, may be biased due to uncertainties in the nuclear data used. For its fusion programmes, the UK aims to meet LLW criteria (less than 12 MBq/kg of β/γ activity) for most of the RW at 100 years after permanent reactor shutdown. However, it has been predicted that some parts of future fusion reactors are likely to result in significant volumes of waste that would be classified as ILW, even after 100 years after end-of-life (EOL), requiring costly geological disposal [2, 3, 4].

To mitigate neutron activation of structural steels used in fusion environments as much as possible, reduced activation ferritic/martensitic (RAFM) steels - such as Eurofer [5] and F82H [6] - have been developed for several decades. The application of RAFM steels aims to uphold the necessary physical properties delivered by conventional structural steels, while reducing neutron activation and hence the amount of RW. To achieve this, the use of alloying elements known to be susceptible to activation (such as Ni, Cu, Nb, Mo) is reduced as much as possible, using less critical elements, such as V, W and Ta, instead [7].

Bailey et al. [8] previously found RAFM steels to activate much less than conventional steels. Of the non-reduced activation FM steels, G91 was least prone to activation, which will partly be subject to study here. Another relevant structural steel is the austenitic stainless steel SS316L(N)-IG (hereon referred to as SS316), which will be used extensively for in-vessel structures of ITER [9, 10] – it is also the primary nuclear steel being considered for the vacuum vessel of the future EU DEMOnstrational power plant (EU-DEMO) [2]. However, due to its high Ni-content, SS316 is highly susceptible to neutron activation, and LLW classification of such a VV under

UK criteria is challenging within 100 years of EOL [11, 12, 13].

As existing predictions on waste classifications and activity levels after reactor EOL are mostly based on modelling and simulation, it is crucial to provide corresponding uncertainty and sensitivity data. Sensitivity data provides insight to which factors of the model have the largest effect on the quantity of interest, whereas uncertainties provide information on the accuracy and hence reliability of a result. This information can subsequently be used to calculate necessary safety margins for quantities such as safe reactor operating times, shielding requirements as well as activity levels of produced RW within the reactor lifetime. Such known uncertainties can then be accounted for in the estimation of operational costs and the necessary handling/disposal of RW. Although previous studies have investigated the effects of uncertainties in nuclear data [16, 17], upon which the majority of activation studies are based, these analyses are generally separated, complicating the direct utilisation of sensitivity and uncertainty results.

Using computational methods, this study aims to model and compare the neutron activation of four structural steels, which are being considered for application in future fusion power plants. The steels of interest are the FM steel G91 (T2), the austenitic stainless steel SS316L(N)-IG, as well as two RAFM steels: Eurofer and F82H. Subsequently, an independent sensitivity and uncertainty analysis was carried out to study the impact of calculation uncertainty on the activation and subsequent waste classifications. The objective of the work is to exemplify a rigorous methodology by which uncertainties can be included in predictions of the neutron-induced response of fusion materials, which can be applied to subsequent engineering design applications.

2. Methodology

2.1. Transport Simulations

Neutron transport simulations were performed using the Monte Carlo code OpenMC (with ENDF/B-VII.1) [14] to obtain a neutron energy flux spectrum for each steel at a given position. Simulations were based on a simplified, spherical, one-dimensional reactor model, the cross-section of which is shown in Figure 1. An isotropic neutron source with an average energy of 14.1 MeV was positioned at the centre of the reactor. The blanket configuration and material compositions were based on a helium-cooled pebble bed (HCPB) design [15] for EU-DEMO, summarised in Table 1. The standard homogenised DEMO HCPB configuration consists of an armour and first wall (FW), followed by layers for the breeding module (BM), backplates and back support structure (BSS). Note that this model does not reflect the actual engineering design, which would be considerably more complex, but rather approximates the variation in material through the thickness of the blanket using mixed average compositions (following table 1). This study compares the activation of Eurofer, F82H and G91 in the FW and the outermost layer (5 cm) of the BSS. In all cases, SS316 was assumed for the VV. In the reactor model, the neutron spectra were tallied in cell tallies, where cells were defined as concentric spheres with a maximum layer width of 5 cm. A total of three simulations were run (one for each option of in-vessel structural material), with 10^{10} neutron histories each. This was judged to be sufficient to ensure good statistical coverage for all the tallies of interest (based on prior experience with similar simulations).

Component	Armour	First Wall	Breeding Module	Backplates	BSS	Vacuum Vessel
Thickness (cm)	0.2	2.5	52	8.5	60	6

Figure 1: 1D reactor model employed in neutron transport simulations using OpenMC.

Table 1: Employed reactor wall configuration as of the HCPB design.

Material (vol.%)	Armour	FW	BM	Backplates	BSS	VV
Tungsten	100	-	-	-	-	-
Eurofer/F82H/G91	-	65	10	41	61	-
Beryllium	-	-	37	-	-	-
Li_4SiO_4	-	-	15	-	-	-
Helium	-	35	38	59	39	-
SS316	-	-	-	-	-	100

2.2. Inventory Simulations

The above transport simulations were followed by a series of inventory calculations with FISPACT-II (version 5.0) [16] to simulate activity as a function of time and identify the dominant radio-nuclides in each material. The elemental compositions of all evaluated steels are summarised in Table A.9 in the appendix. The FISPACT-II simulations used the TENDL-2017 database of nuclear reaction data and the OpenMC-calculated neutron flux spectra, where the spectra were converted from their original *neutron cm/source neutron* units to *neutrons/cm*^{2}*s* units assuming a first wall neutron loading of 2 MWm^{-2}. Irradiation was simulated for 4 hours per day for 20 years, and subsequent $(\beta + \gamma)$-activities were evaluated from shut-down up to 200 years after EOL, with the dominant (highest activity) nuclides identified from the evolving inventory as a function of time.

2.3. Sensitivity and Uncertainty Analysis

The sensitivity and uncertainty analysis (SUA) was carried out separately from any inventory calculations, using the deterministic code package XSUN-2022 [17], including TRANSX-2.15 [18, 19] for the preparation of multi-group nuclear cross-sections, the discrete-ordinate (S_N) transport code PARTISN-5.97 [20, 21], and SUSD3D [22, 23] for the final nuclear data sensitivity and uncertainty calculations. The XSUN-2022 code system involves a complete set of the deterministic codes mentioned above, with the internal data processing shown in Figure 2. Note that in PARTISN, the Vitamin-J 175-energy group structure was used, with the same 1D-reactor configuration that was used as in Section 2.1. Sensitivities were calculated using Generalised Perturbation Theory. Reaction rates for the production of nuclides were calculated via:

$$RR = \sum_g \sigma_g^D \Phi_g \tag{1}$$

Here, σ_g^D is the response function for the nuclide generation reaction in the energy group g, and Φ_g is neutron flux. The corresponding uncertainties were obtained

from the sandwich equation:

$$(\Delta RR)^2 = S^T \cdot Cov \cdot S \tag{2}$$

where S and S^T represent the sensitivity vector of the reaction rate to groupwise cross sections and its transpose, respectively, and Cov is the corresponding cross section covariance matrix.

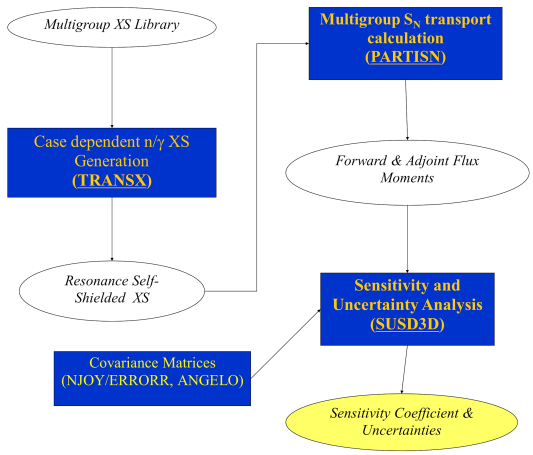

Figure 2: Work chain of XSUN-2022 code system [17].TRANSX was used to process nuclear data into transport tables compatible with deterministic codes. With PARTISN, the Boltzmann Transport Equation was solved for direct and adjoint flux. ANGELO and NJOY were used for covariance matrix processing. SUSD3D performed the SUA using first order generalized perturbation theory.

The activity level $A(t)$ at a given time t, is calculated as the sum of contributions from all decaying nuclides i using their concentrations at the end of operation, viz

$$A(t) = \sum_i N_{0i} \lambda_i \mathrm{e}^{-\lambda_i t} \tag{3}$$

Taking into account the uncertainty in nuclide production, this activity becomes:

$$A(t) = \sum_i N_{0i}(1 \pm \Delta_i) \lambda_i \mathrm{e}^{-\lambda_i (t \pm \Delta t)} \tag{4}$$

where Δ_i is the uncertainty (from XSUN-2022) in the production of a given radionuclide. Here we define Δt as the delay in reaching a specified activity level (such as the UK LLW limit of 12 MBq/kg) associated with the uncertainty. FISPACT-II activity results from close to the target activity were used to interpolate (in general it is not possible to fit exactly the activity decay curves as there may be contributions from multiple nuclides with different half-lives) the range of 'time-to-target' values (min, max) and hence to obtain Δt.

If $i = 1$, i.e. there is only one dominant nuclide in a material, the time delay Δt due to an uncertainty Δ can be calculated analytically. We have, in this case:

$$\frac{N(t)}{N_0(1 \pm \Delta)} = \mathrm{e}^{-\lambda(t \pm \Delta t)}, \tag{5}$$

where $A(t) = N(t)\lambda$ and

$$\pm \Delta t = \frac{\ln(1 \pm \Delta)}{\lambda} \tag{6}$$

For every assessed steel, an independent sensitivity and uncertainty analysis was conducted for each dominant nuclide contributing above 15% to the total material activity, as identified from the FISPACT-II results (see Tables 2 and 3). For Eurofer, F82H and G91 this was carried out in the front (FW) and the back (BSS) of the reactor wall. For SS316, the sensitivity and uncertainty analysis was performed in the VV. Note that any uncertainties calculated by FISPACT-II only include those associated with the decay constants (λ) and transmutation cross-sections (σ) [16]. The results from XSUN-2022 include uncertainties in the transmutation reaction-rates (response functions) as well as uncertainties propagated from transport cross-sections (i.e. uncertainty contributions from all nuclide cross-sections which impact neutron transport through the reactor). To ensure compatibility between FISPACT-II and XSUN-2022, nuclear data from TENDL-2017 [24] were used for response functions (i.e. SUSD3D used the same data as FISPACT-II for transmutation reactions), whereas JEFF-3.3 [25], which is the reference cross section evaluation in XSUN-2022, was used for transport cross-sections. For cases where the uncertainty is dominated by the response function, values of uncertainties are therefore similar for FISPACT-II and XSUN-2022 results. Note that uncertainties from FISPACT-II are only displayed for total material activity. It is emphasised that the uncertainty analysis conducted using the XSUN-2022 package only encompasses uncertainties on nuclear cross-section data, not on decay data.

The individual uncertainties in nuclide production cross-sections were used to calculate a lower and upper bound for the amount of each dominant nuclide present in a material, which was then used to define a range of possible material concentrations at the end of operation. These altered compositions were used in FISPACT-II calculations to define the range in activities of each material from which the minimum and maximum 'time-to-reach LLW' was obtained via interpolation (as described above).

3. Results and Discussion

3.1. Neutron Activation and Waste Categorization Results

Figure 3 shows the total activity of all in-vessel steels 100 years after EOL, as a function of distance through the outboard reactor wall. In each material case, LLW

criteria were not met for large proportions of the blanket. For the RAFM steels (Eurofer and F82H), a transition from ILW to LLW activity level was observed approximately half-way through the reactor wall, whereas G91 exceeded those limits almost entirely. For all cases, this mixture of LLW and ILW material within components may complicate the decommissioning process.

At the FW (1.45 cm depth), the activity of Eurofer was over an order of magnitude higher than the LLW limit of 12 MBq/kg. F82H exhibited the best resistance to neutron activation throughout, but is still predicted to be activated to over six times the LLW limit at the FW, whereas G91 activity exceeded the LLW limit by more than two orders of magnitude at 100 years.

As expected, material activation decreased as a function of distance through the reactor wall due to decreasing neutron fluxes. Activation of Eurofer resulted in ILW at 100 years until the backplate; from approximately 60 cm depth, activity was below the LLW limit at 100 years. For F82H, LLW at 100 years was achieved after about 54 cm (within the BM). G91 performed much worse, with activity only falling below the LLW limit after approximately 115 cm (BSS).

In the outermost 5 cm of the BSS, all in-vessel steels categorise as LLW at 100 years. One could argue that it may be more suitable to use RAFM steels closer to plasma-facing components, whereas the advantage of reduced activation is less apparent in the far back. Hence, the use of different (non-RAFM) steels may be more viable in those regions.

The total activity of the VV (SS316) (see Table 8) varied with the kind of steel used in the blanket structure. In each case, VV activity exceeded LLW criteria at 100 years after shutdown, reaching 8.05×10^7 Bq/kg, 8.03×10^7 Bq/kg and 9.85×10^7 Bq/kg for the in-vessel steel cases of Eurofer, F82H and G91, respectively. As described in sections 3.1.1 and 3.1.2, the activated nuclides responsible for elevated radioactivity vary between the FW and BSS, even within the same kind of steel.

3.1.1. First Wall

Table 2 summarises the dominant nuclides with highest contributions to total steel activity in the FW at 100 years after EOL. Only nuclides contributing more than 15% to total material activity at this time are listed with their relevant production pathways. The production pathway analysis was performed using a tree search algorithm in FISPACT-II, see [16] for more details.

The high activity of Eurofer at 100 years after permanent reactor shutdown is due to several nuclides; ^{121m}Sn, ^{121}Sn, ^{63}Ni and ^{14}C. In F82H, by contrast, ^{63}Ni was the only dominant nuclide identified, being responsible for about two thirds of the

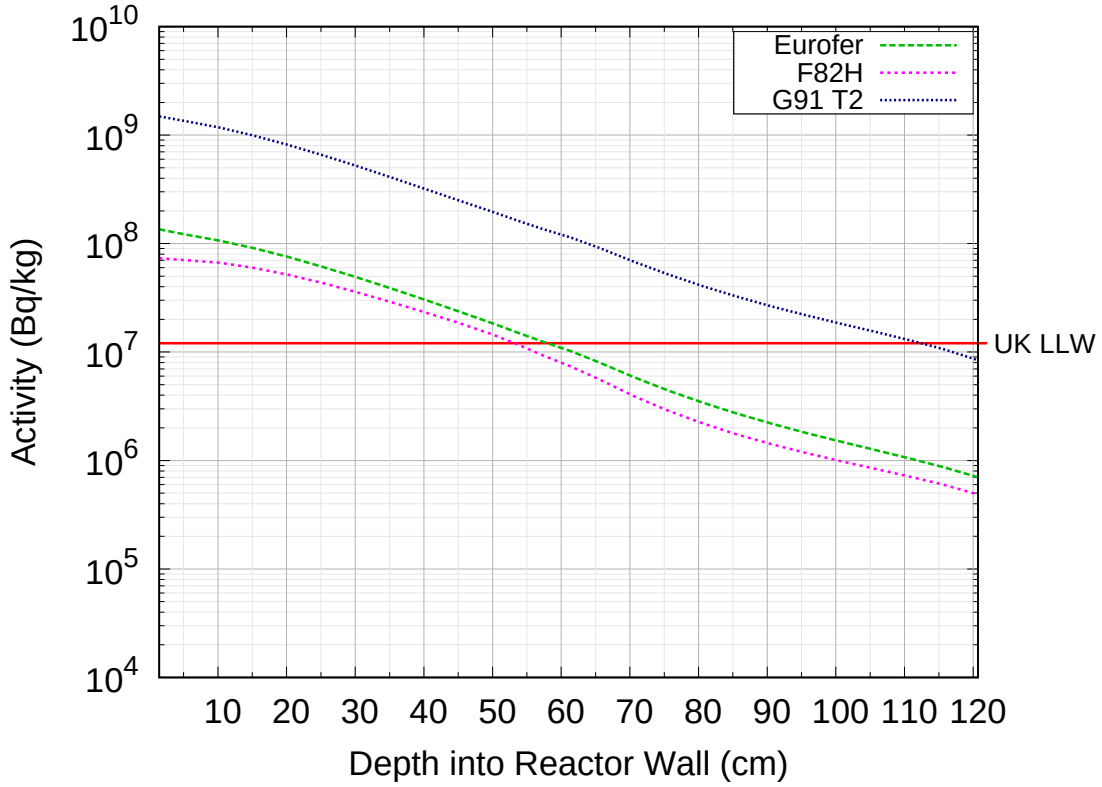

Figure 3: Total activity of in-vessel materials at 100 years after reactor EOL as a function of depth through the reactor wall, moving radially outwards.

total activity (with minor contributions from a number of other radionuclides - see Figure 5). This is in accordance with their respective compositions, as Eurofer contains 50 times the amount of tin compared to F82H and six times more nitrogen than F82H, whereas F82H has triple the amount of nickel. ^{63}Ni is also a dominant nuclide in G91, in addition to ^{91}Nb, which make up approximately 27% and 37%, respectively, of total G91 activity 100 years after EOL. Niobium is an element known to cause activity-related problems and is therefore commonly minimised in RAFM steels; ^{91}Nb has a half-life of 680 years. With 0.1 wt.%, the Nb-content in G91 is 20 times higher than in Eurofer, and 2000 times that of F82H.

The production pathways in Table 2 show the nuclear reaction cross-sections on which the sensitivity and uncertainty analyses were performed for the FW; the results are presented in Section 3.2.

Figure 4 displays the total material activity for Eurofer in the FW from EOL to 200 years after shutdown, including relative contribution to activities (top graph)

Table 2: Summary of all radio-nuclides produced through neutron activation in the FW, contributing a minimum of 15% to the overall material activity at 100 years after EOL. The pathway percentage indicates the amount of radio-nuclide produced though the given nuclear reaction.

Steel	**Dominant Nuclide**	**Contribution to Activity**	**Half-life**	**Production Pathway**	**Pathway Percentage**
Eurofer	^{121m}Sn	26.5%	44 years	^{120}Sn(n,γ)^{121m}Sn	26.4%
				^{122}Sn(n,2n)^{121m}Sn	62.9%
	^{121}Sn	20.6%	27 hours	^{120}Sn(n,γ)^{121}Sn	81.4%
				^{122}Sn(n,2n)^{121}Sn	7.7%
	^{63}Ni	18.1%	101 years	^{62}Ni(n,γ)^{63}Ni	36.8%
				^{63}Cu(n,p)^{63}Ni	56.5%
	^{14}C	15.7%	5705 years	^{14}N(n,p) ^{14}C	99.9%
F82H	^{63}Ni	66.8%	101 years	^{62}Ni(n,γ)^{63}Ni	52.6%
				^{63}Cu(n,p)^{63}Ni	35.0%
G91	^{91}Nb	37.0%	680 years	^{92}Mo(n,np)^{91}Nb	83.9%
				^{92}Mo(n,2n)^{91}Mo(β+)^{91}Nb	14.6%
	^{63}Ni	26.7%	101 years	^{62}Ni(n,γ)^{63}Ni	46.5%
				^{63}Cu(n,p)^{63}Ni	42.9%

of individual dominant nuclides. At EOL, dominant nuclides are ^{55}Fe as well as other nuclides, such as ^{54}Mn and ^{182}Ta, originating from the base and main alloying elements. Due to their relatively short half-lives, the significance of their activity decreases with time, whereas the relative contributions of other nuclides increase. Activity levels 100 years after EOL were approximately an order of magnitude above the LLW limit, due to the combined activity of ^{121m}Sn, ^{121}Sn, ^{63}Ni and ^{14}C, contributing between approximately 16 - 27% each (see Table 2).

FW activity of F82H is shown in Figure 5 for the same time period. At EOL, dominant nuclides are ^{55}Fe ^{60}Co, ^{3}H, which cross-over with ^{63}Ni at about 60 years. The half-life of ^{63}Ni is approximately 100 years, and is largely responsible for exceeding LLW limits at 100 years after EOL. Although the elemental composition of F82H contains less tin and nitrogen, its higher nickel content shifts the relative nuclide contribution to activity from several to just one dominant nuclide.

Figure 6 shows activity of G91 in the FW. Similarly to Eurofer and F82H, the main initial activity is due to ^{55}Fe, produced from neutron capture of ^{54}Fe. At about 50 years after EOL, almost two thirds of its activity are accounted for by ^{63}Ni and ^{91}Nb. Nuclides that never contribute more than 10% of the total activity during the 200 years of decay are not plotted separately in Figures 4 to 6 but instead their activities are summed together as the "other" curve in the plots. Note that the individual uncertainties in their production cross-sections are assumed to be uncorrelated.

It is apparent that, in the FW, neither Eurofer, nor F82H or G91 reach LLW activity levels within the displayed 200 years, where the activity of G91 is over two orders of magnitude above the RAFM steels. In fact, it was found that these structural steels exceeded LLW limits for over 750 (F82H) or even 1000 years (Eurofer, G91). This is problematic since, even with the use of RAFM steels, ILW disposal will most likely not be preventable.

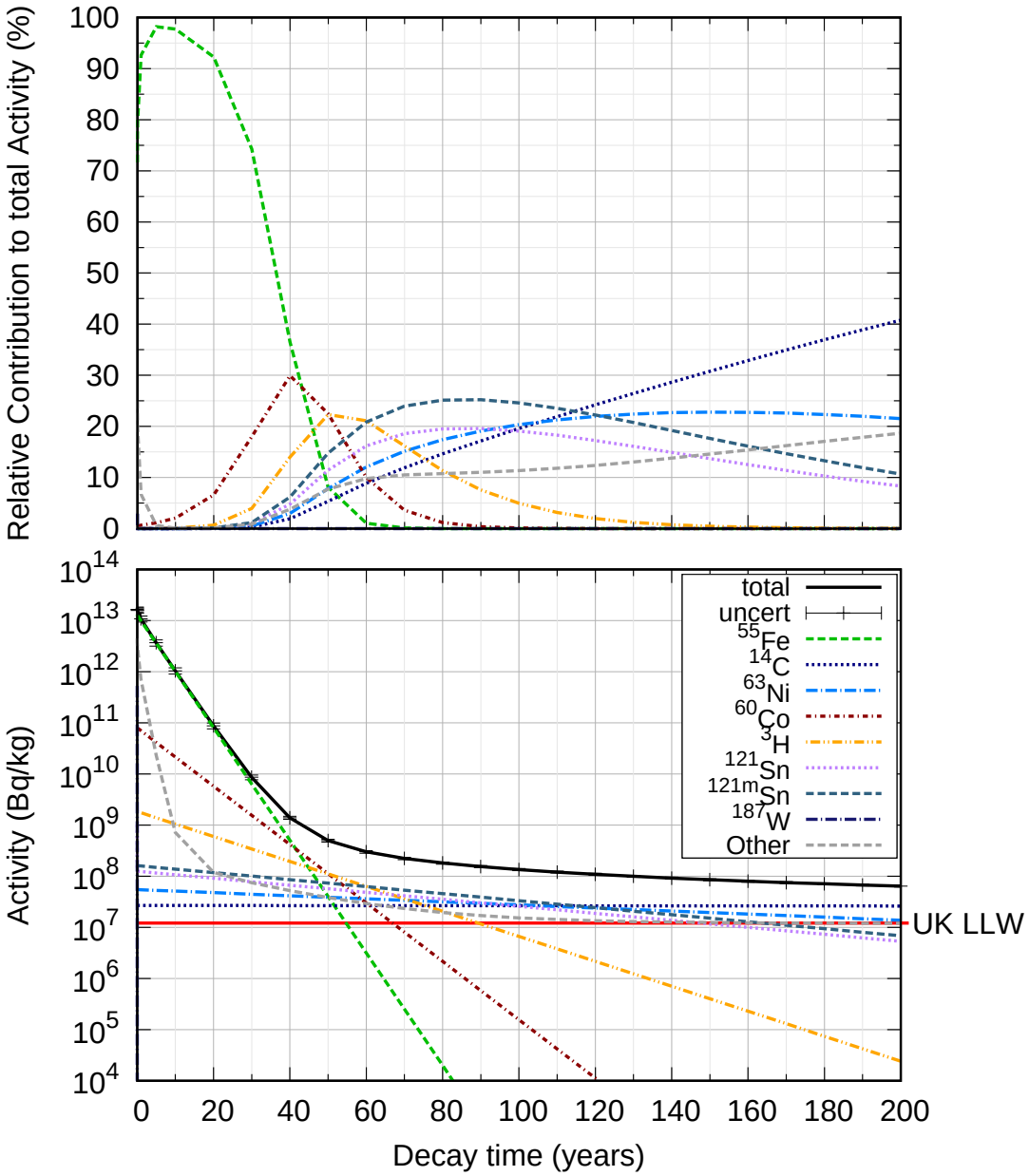

Figure 4: (Top): %-Contribution of dominant nuclides to total activity of Eurofer from EOL to 200 years in the FW. (Bottom): Total activity of Eurofer at FW. Nuclides are only displayed if they contributed more than 10% at any point in the decay. The "other" curve is the sum of nuclides which do not meet this criteria; they include ^{54}Mn and ^{182}Ta among others.

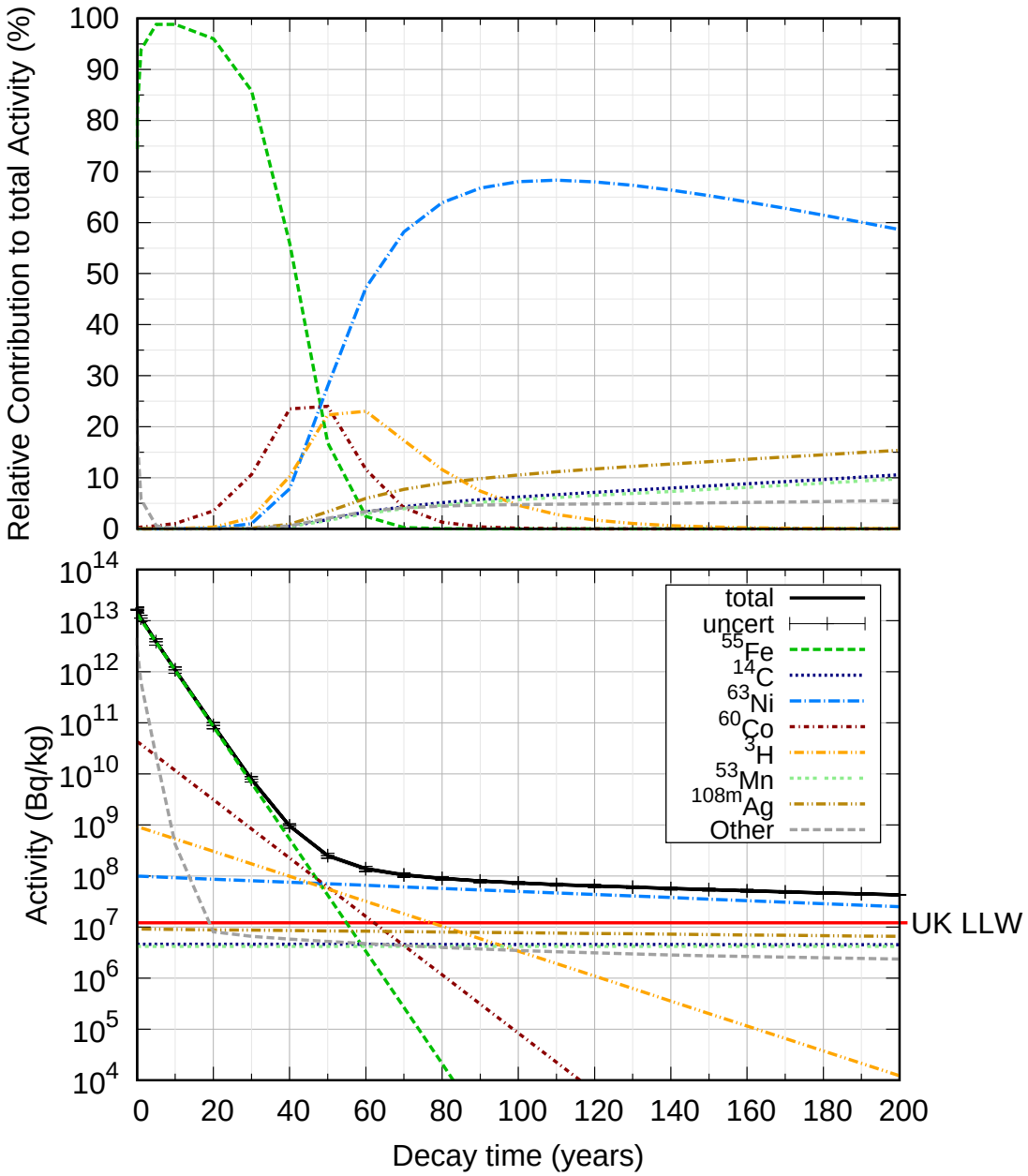

Figure 5: (Top): %-Contribution of dominant nuclides to total activity of F82H from EOL to 200 years.(Bottom): Total activity of F82H at FW. Nuclides are only displayed if they contributed more than 10% at any point in the decay. The "other" curve is the sum of nuclides which do not meet this criteria; they include ^{121,121m}Sn and ^{108}Ag among others.

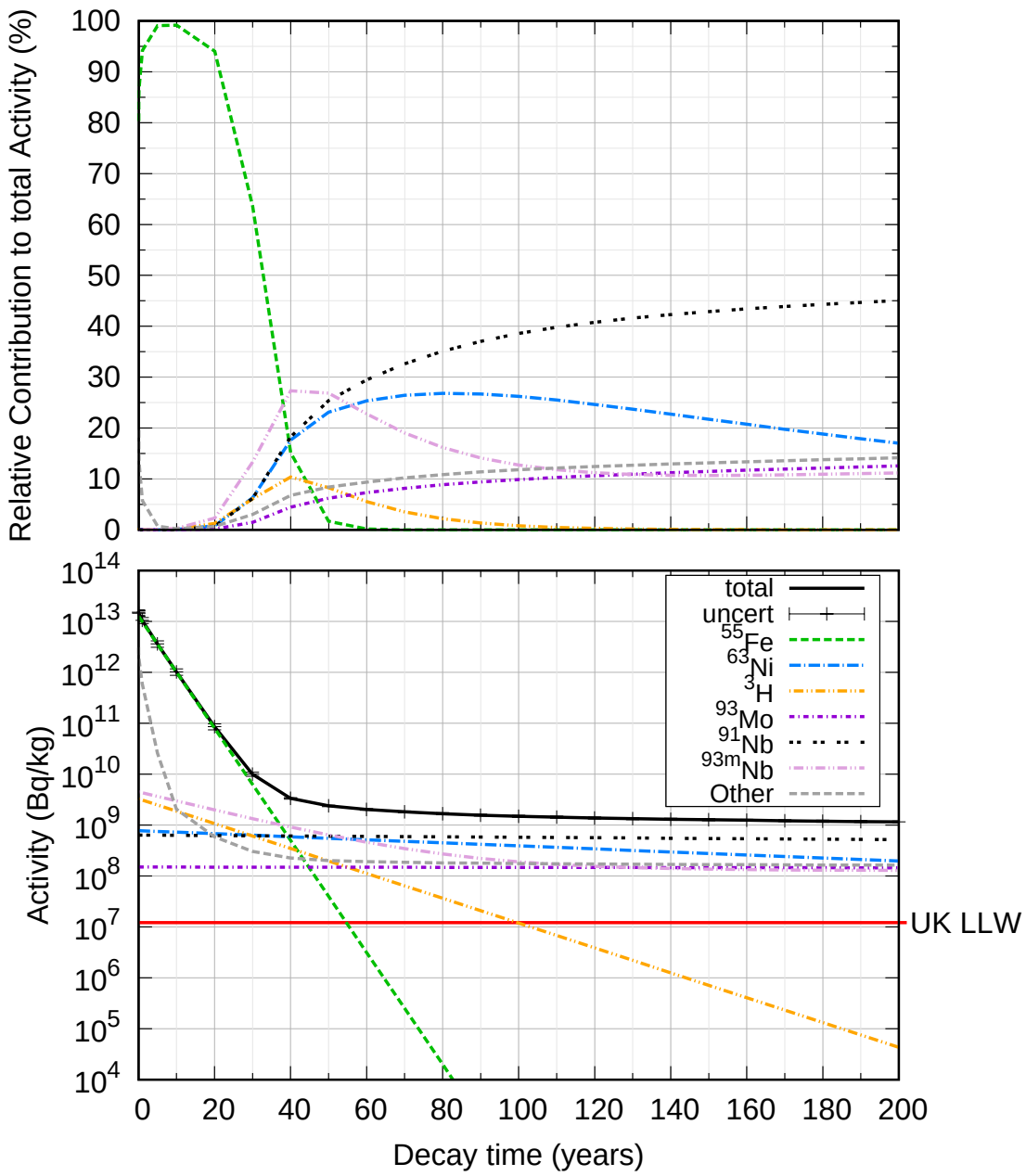

Figure 6: (Top): %-Contribution of dominant nuclides to total activity of G91 in FW from EOL to 200 years. (Bottom): Total activity of G91 at FW. (Bottom): Total activity of F82H at FW. Nuclides are only displayed if they contributed more than 10% at any point in the decay. The "other" curve is the sum of nuclides which do not meet this criteria; they include ^{94}Nb, ^{14}C and ^{60}Co among others.

3.1.2. BSS and VV

The identified dominant radio-nuclides in the BSS are summarised in Table 3. Since the BSS reaches LLW limits much earlier than 100 years after EOL, the dominant nuclides are given for 20 years after EOL. Due to the drastic change in neutron energies incident on the material in the BSS compared to the FW, other nuclear cross-sections dominate radio-nuclide production in the BSS. The main nuclides responsible for material activity in the BSS are ^{55}Fe and ^{60}Co in Eurofer and F82H, where they make up 99.5% of material activity at 20 years after EOL in Eurofer and 99.9% in F82H. G91 does not contain any cobalt, so at 20 years 97.8% of its activity is solely due to ^{55}Fe. Figures 7 to 9 show the absolute activities as well as the relative nuclide contributions for Eurofer, F82H and G91 activity in the BSS from EOL to 200 years. These results were obtained from the outermost 5 cm of the BSS, where all in-vessel steels met LLW the criteria within 100 years. In this regime, LLW is reached within approximately 30 to 45 years after shutdown.

The activity of the VV is shown in Figure 10 from EOL to 200 years after (data shown corresponds to neutron spectra obtained with Eurofer as in-vessel steel). As the VV is made of austenitic stainless steel 316, the high Ni-content of 12.5 wt.% leads to significant activation. ^{63}Ni is the dominant nuclide in the VV, with its contribution to total activity varying slightly with the in-vessel steel used. With contributions of 92.5%, 92.7% and 93.7% for Eurofer, F82H and G91, respectively, it is obvious that ^{63}Ni is solely responsible for the failure of the VV to meet LLW requirements 100 years after EOL. Initially, activity is dominated by ^{55}Fe and ^{60}Co, but as their half-lives are only 2.7 and 5.2 years, respectively, ^{63}Ni starts to dominate material activity after approximately 30 years, accounting for up to 93% of total VV activity at 80 years post EOL. As can be seen in the bottom part of Figure 10, the total activity curve follows the ^{63}Ni-line closely from 60 years onwards. To successfully reduce activation of the VV, ^{63}Ni-production must be prevented either by employment of a different material or by providing sufficient shielding of the VV, which poses a variety of challenges.

Figure 11 shows the neutron flux profile across the VV of 6 cm thickness. The data is presented corresponding to the 709-group energy-bin structure, as used in FISPACT-II, which is a high-resolution grid where the bins are approximately equidistant on a logarithmic scale. The highest energy peak above 10^7 eV represents the direct 14 MeV neutrons from the fusion reaction. In the low and thermal energy regions, the neutron flux in the VV is much higher if the in-vessel steel used is G91, compared to the RAFM steels. This difference in flux is responsible for the difference in VV activities between each blanket material case. The flux for Eurofer is also slightly higher than for F82H in this region, which is in agreement with the resulting higher VV activity after 100 years. This suggests that the RAFM steels not only suffer

from less neutron activation, but they render a better shielding performance against fusion neutrons than G91 [26].

Table 3: List of all radio-nuclides produced through neutron activation in the BSS, contributing a minimum of 15% to the overall material activity at 20 years after EOL. The pathway percentage indicates the amount of radio-nuclide produced though the given nuclear reaction.

Steel	**Dominant Nuclide**	**Contribution to Activity**	**Half-life (years)**	**Production Pathway**	**Pathway Percentage**
Eurofer	^{55}Fe	71.1%	2.74	^{54}Fe(n,γ)^{55}Fe	89.5%
	^{60}Co	28.4%	5.27	^{59}Co(n,γ)^{60}Co	99.9%
F82H	^{55}Fe	83.3%	2.74	^{54}Fe(n,γ)^{55}Fe	89.3%
	^{60}Co	16.6%	5.27	^{59}Co(n,γ)^{60}Co	99.9%
G91	^{55}Fe	97.8%	2.74	^{54}Fe(n,γ)^{55}Fe	91.3%

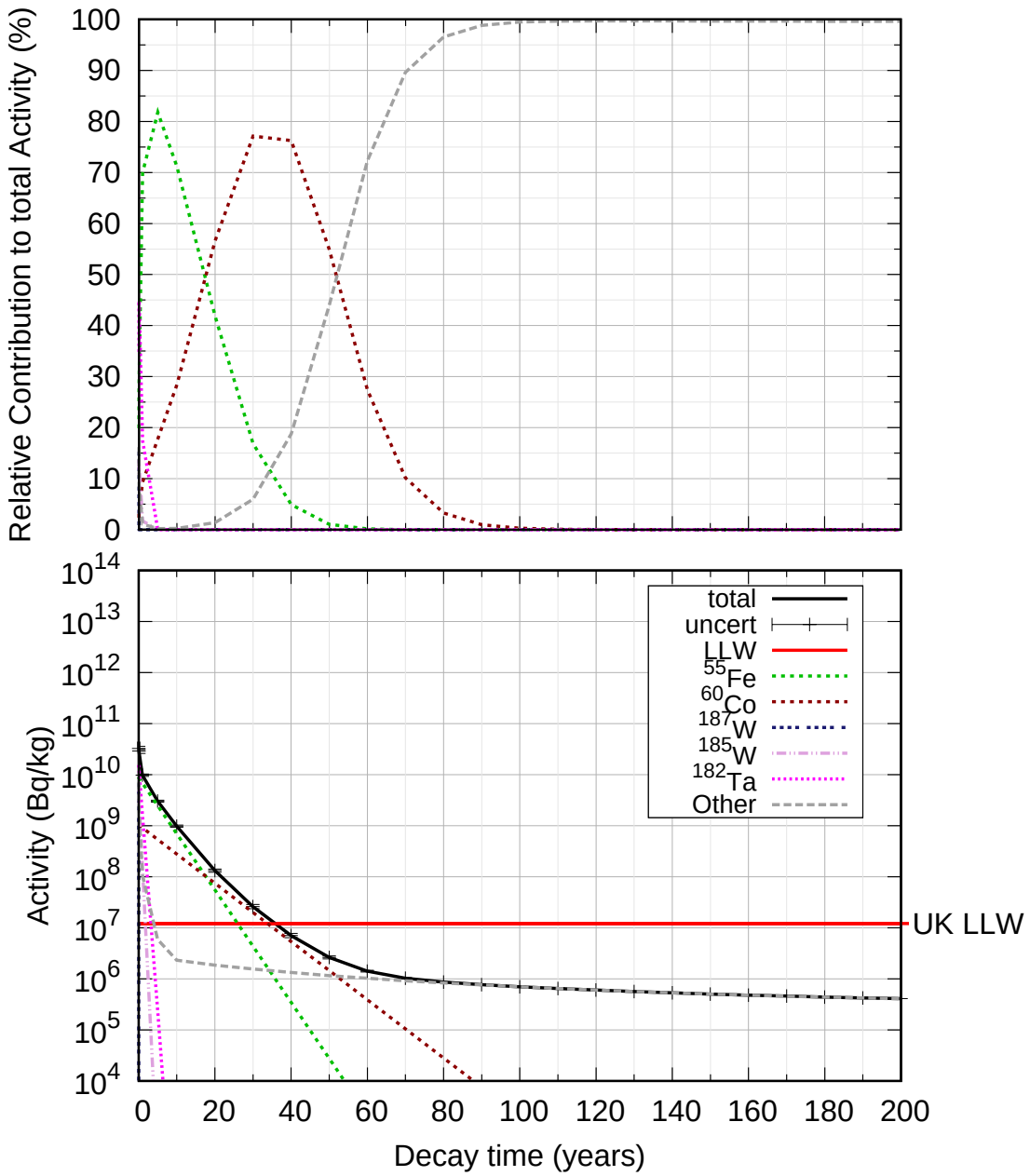

Figure 7: (Top): %-Contribution of dominant nuclides to total activity of Eurofer in BSS from EOL to 200 years. (Bottom): Total activity of Eurofer from EOL to 200 years. Nuclides are only displayed if they contributed more than 10% at any point in the decay. The "other" curve is the sum of nuclides which do not meet this criteria; they include and ^{14}C, ^{121,121m}Sn and ^{63}Ni among others.

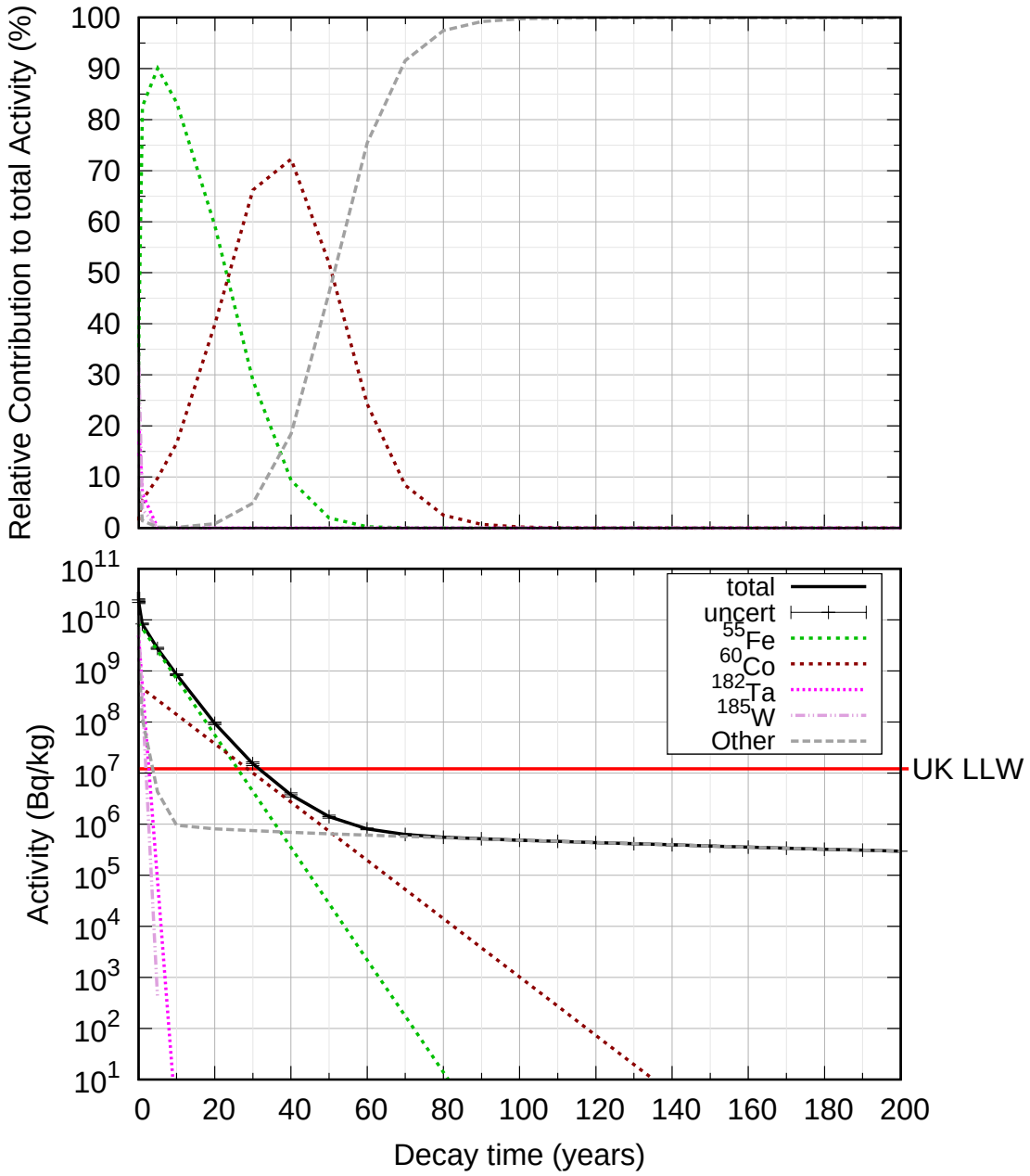

Figure 8: (Top): %-Contribution of dominant nuclides to total activity of F82H in BSS from EOL to 200 years. (Bottom): Total activity of F82H from EOL to 200 years. Nuclides are only displayed if they contributed more than 10% at any point in the decay. The "other" curve is the sum of nuclides which do not meet this criteria; they include and ^{187}W, ^{108m}Ag and ^{63}Ni among others.

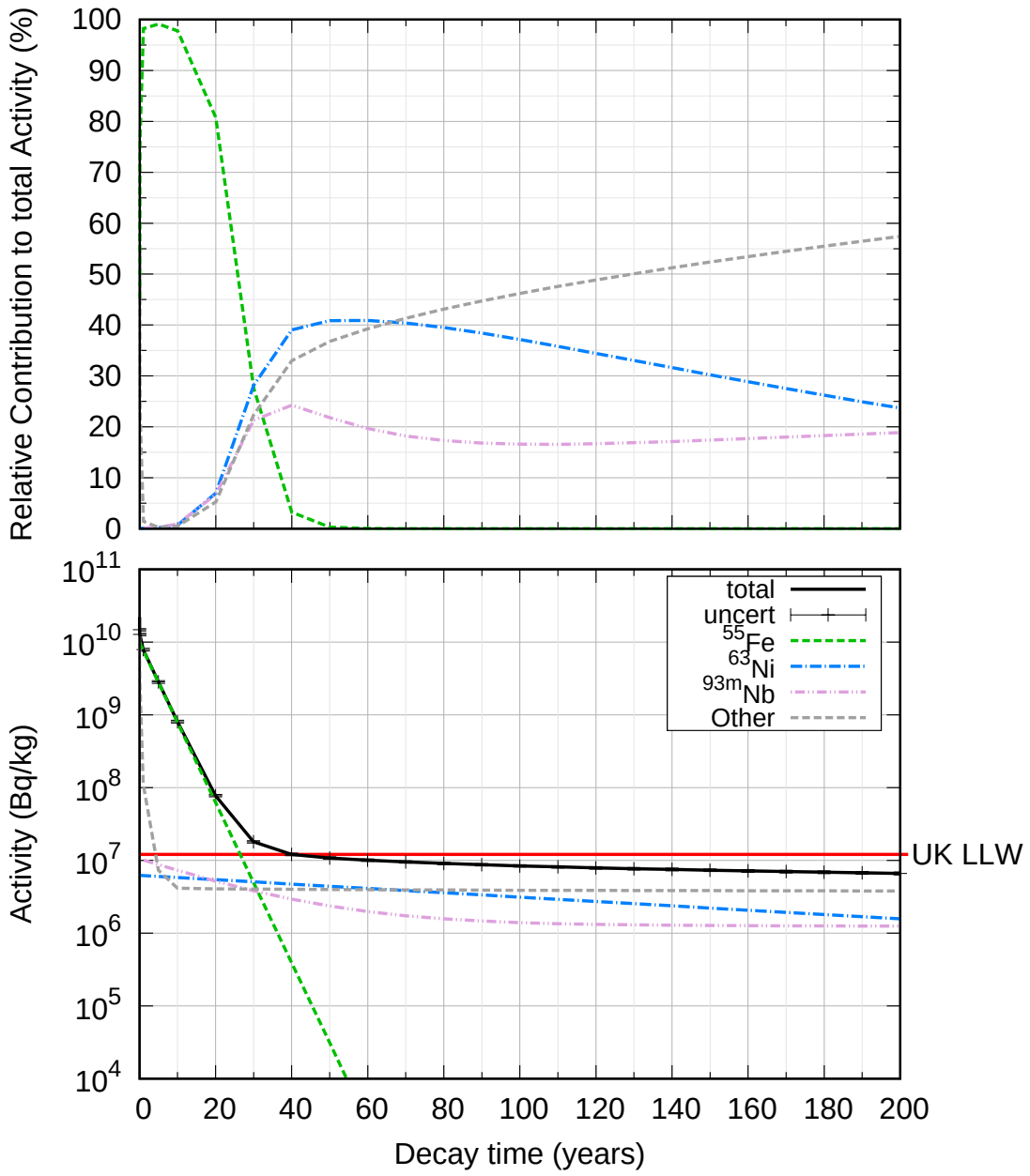

Figure 9: (Top): %-Contribution of dominant nuclides to total activity of G91 in BSS from EOL to 200 years. (Bottom): Total activity of G91 from EOL to 200 years. Nuclides are only displayed if they contributed more than 10% at any point in the decay. The "other" curve is the sum of nuclides which do not meet this criteria; they include and ^{187}W, ^{94}Nb and ^{59}Ni among others.

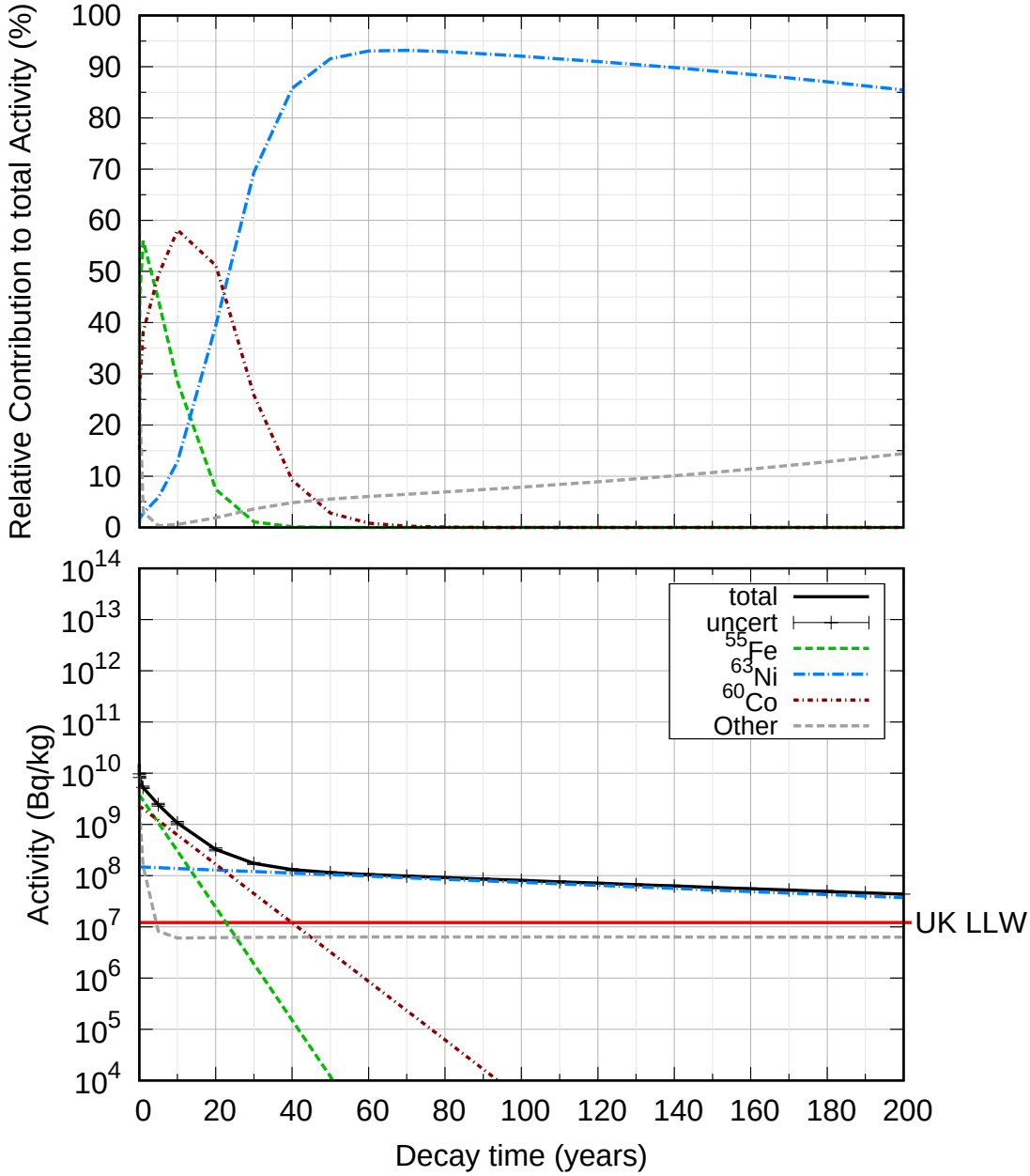

Figure 10: (Top): %-Contribution of dominant nuclides to total activity of SS316 in VV from EOL to 200 years (using data from simulations with Eurofer as the in-vessel steel). (Bottom): Total activity of SS316 from EOL to 200 years. "Other" displays the sum of any individual radionuclides contributing less than 10% to the total material activity at any point within the plotted time period, which include ^{93}Mo, ^{59}Ni and ^{93m}Nb among others.

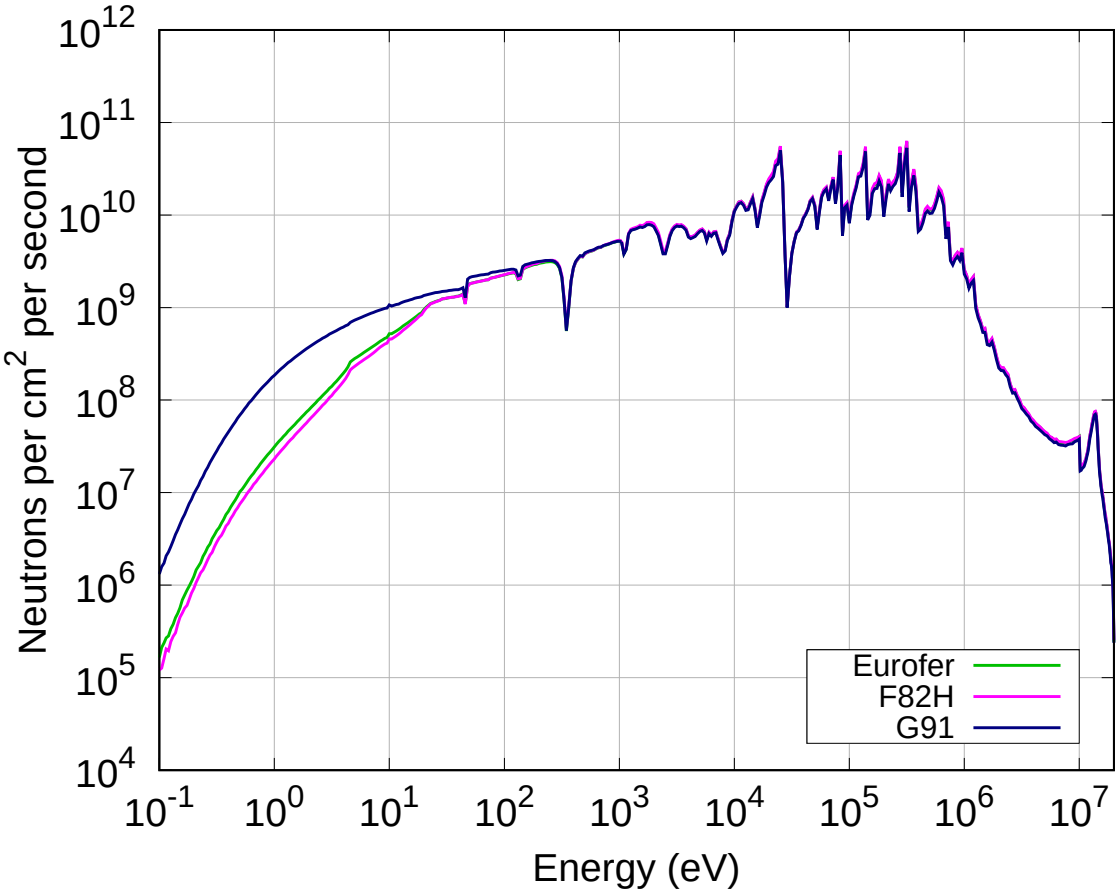

Figure 11: Neutron energy profile across the VV (SS316), shown for each in-vessel material.

3.2. Sensitivity and Uncertainty Results

For the dominant nuclides identified for each assessed steel in the FW, BSS and VV, a sensitivity and uncertainty analysis was carried for each production pathway. Table 4 lists the uncertainties for each dominant nuclide production cross-section in the FW and BSS. For the same nuclear cross-section, uncertainties are generally higher in the BSS than in the FW. This is the case for the ^{62}Ni(n,γ)^{63}Ni reaction in G91, where the uncertainty increases from 0.8% to 3.3%. In regions closer to the source (FW), uncertainties are dominated by uncertainties in the transmutation cross-sections, whereas in the deeper blanket regions (BSS), the contribution of transport cross-sections (such as collisions with nuclides of other blanket materials) increases. However, a direct comparison is not possible with the remaining data shown, as the dominant nuclide and hence their production pathways (cross-sections) change between front and back-end of the blanket, which is due to a change in shape of the neutron flux spectrum.

Table 4: Uncertainty contributions for the main production pathways of the identified dominant nuclides for each steel assessed in the FW and BSS. For SUSD3D, the combined uncertainties come from JEFF-3.3 and are based on the total uncertainty impact on the identified reaction channel from transport and transmutation uncertainties.

Region	**Steel**	**Dominant Nuclide**	**Production Cross-section**	**SUSD3D Uncertainty**	
				combined[1]	response[3]
FW	Eurofer	^{121}Sn	^{120}Sn(n,γ)^{121m}Sn	0.9%	0%[2]
			^{122}Sn(n,2n)^{121m}Sn	11.1%	11.0%
		^{63}Ni	^{62}Ni(n,γ)^{63}Ni	1.4%	0%
			^{63}Cu(n,p)^{63}Ni	2.1%	2.0%
		^{14}C	^{14}N(n,p)^{14}C	0.4%	0%[2]
	F82H	^{63}Ni	^{62}Ni(n,γ)^{63}Ni	0.9%	0%
			^{63}Cu(n,p)^{63}Ni	2.2%	2.0%
	G91	^{91}Nb	^{92}Mo(n,2n)^{91}Mo(β^+)^{91}Nb	23.8%	23.8%[3]
			^{92}Mo(n,np)^{91}Nb	0.5%	0%[2]
		^{63}Ni	^{62}Ni(n,γ)^{63}Ni	0.8%	0%[2]
			^{63}Cu(n,p)^{63}Ni	2.1%	1.9%
BSS	Eurofer	^{55}Fe	^{54}Fe(n,γ)^{55}Fe	28.5%	28.4%
		^{60}Co	^{59}Co(n,γ)^{60}Co	3.8%	0%[2]
	F82H	^{55}Fe	^{54}Fe(n,γ)^{55}Fe	28.1%	28.0%
		^{60}Co	^{59}Co(n,γ)^{60}Co	3.9%	0%[2]
	G91	^{55}Fe	^{54}Fe(n,γ)^{55}Fe	28.3%	28.1%
		^{63}Ni	^{62}Ni(n,γ)^{63}Ni	3.3%	0%[2]
		^{93m}Nb	^{93}Nb(n,n')^{93m}Nb	10.0%	9.0%

[1] Uncertainty due to both transport (JEFF-3.3) and transmutation (TENDL-2017) cross-sections

[3] Uncertainty due to transmutation (response) TENDL-2017 cross-sections only

[2] Covariance matrices not available in JEFF-3.3 / TENDL-2017

[3] Covariance matrices not available in JEFF-3.3 and taken from ENDF/B-VIII.0

TABLE FROM PROOF

Table 5: Uncertainty contributions for the main production pathways of the identified dominant nuclides for each steel assessed in the FW and BSS. For SUSD3D, the combined uncertainties come from JEFF-3.3 and are based on the total uncertainty impact on the identified reaction channel from transport and transmutation uncertainties.

Region	Steel	Dominant nuclide	Production cross-section	SUSD3D uncertainty	
5-6				Combined[a]	Response[b]
FW	Eurofer	121Sn	120Sn(n,γ)^{121m}Sn	0.9%	0%[c]
			122Sn(n,2n)^{121m}Sn	11.1%	11.0%[3pt]
		63Ni	62Ni(n,γ)63Ni	1.4%	0%
			63Cu(n,p)63Ni	2.1%	2.0% [3pt]
		14C	14N(n,p)14C	0.4%	0%[c]
	F82H	63Ni	62Ni(n,γ)63Ni	0.9%	0%
			63Cu(n,p)63Ni	2.2%	2.0%[3pt]
	G91	91Nb	92Mo(n,2n)91Mo(β^+)91Nb	23.8%	23.8%[d]
			92Mo(n,np)91Nb	0.5%	0%[c] [3pt]
		63Ni	62Ni(n,γ)63Ni	0.8%	0%[c]
			63Cu(n,p)63Ni	2.1%	1.9%
BSS	Eurofer	55Fe	54Fe(n,γ)55Fe	28.5%	28.4%
		60Co	59Co(n,γ)60Co	3.8%	0%[c] [3pt]
	F82H	55Fe	54Fe(n,γ)55Fe	28.1%	28.0%
		60Co	59Co(n,γ)60Co	3.9%	0%[c] [3pt]
	G91	55Fe	54Fe(n,γ)55Fe	28.3%	28.1%
		63Ni	62Ni(n,γ)63Ni	3.3%	0%[c]
		^{93m}Nb	93Nb(n,n')^{93m}Nb	10.0%	9.0%

[a]Uncertainty due to both transport (JEFF-3.3) and transmutation (TENDL-2017) cross-sections. [b]Uncertainty due to transmutation (response) TENDL-2017 cross-sections only. [c]Covariance matrices not available in JEFF-3.3/TENDL-2017. [d]Covariance matrices not available in JEFF-3.3 and taken from ENDF/B-VIII.0.

The calculated uncertainties were propagated to evaluate their effect on the average time taken for each assessed steel to reach LLW limits. As described in Section 2.3, values for minimum and maximum time to LLW were calculated for the BSS. The FW activities vastly exceeded UK LLW limits far beyond 100 years after EOL, as summarised in Table 6. F82H exhibited the lowest overall activity in the FW, but was still found to require over 750 years to reach the same activity as the LLW limit, far off the desired 100 years. However, Eurofer and G91 were both found to exceed 1000 years to reach the UK LLW limit of 1.2×10^7 Bq/kg, in agreement with previous works [3, 8].

Table 6: Approximate time taken for activated in-vessel structural steels in the FW to decay to UK LLW waste activity limits. The activity level at 100 years after EOL is also provided.

Steel	**Activity 100 years after EOL (Bq/kg)**	**Time to LLW (years)**
Eurofer	1.35E+08	>1000
F82H	7.33E+07	>750
G91	1.49E+09	>1000

The minimum, mean and maximum time taken to meet LLW levels for the BSS were interpolated using FISPACT-II, with the results listed in Table 7. As F82H exhibited the lowest activity in the BSS and throughout the blanket, the corresponding time to LLW was the shortest. The maximum time to LLW calculated for F82H from the corresponding uncertainties was about 33 years - still more than two years before the earliest possible time predicted for Eurofer to meet LLW levels. However, a mean time of 36 years to LLW for Eurofer is well before the 100-year aim. According to the results of this study, the outermost part of the BSS could reach LLW within 30 years of EOL. This gives a 10-year advantage compared to using G91, which would reach LLW at the earliest within 39.6 years, but may take up to 43 years. Note, that this only assesses the outermost 5 cm of the BSS, and uncertainty values are based on dominant nuclide production only.

Table 7: Approximate time taken for activated steels in the outermost 5 cm of the BSS to decay to LLW waste activity limits. Minimum and maximum required times were calculated from minimum and maximum amounts of dominant nuclides present due to nuclear data uncertainties.

Steel	**Minimum time to LLW (years)**	**Mean time to LLW (years)**	**Maximum time to LLW (years)**
Eurofer	35.2	36.3	37.3
F82H	29.5	31.5	32.9
G91	39.6	40.2	43.0

VV activity levels at 100 years and uncertainties in ^{63}Ni production in SS316 for each in-vessel case are listed in Table 8, along with the corresponding time uncertainties to reach LLW. FISPACT-II results showed that although in each assessed case the VV contained only SS316, employing RAFM steels for the in-vessel structures had a measurable effect, as previously discussed and shown in Figure 11. The activity of SS316 reached with G91 as the blanket structural material was roughly 12-fold of the VV activity behind the assessed RAFM steels used in the blanket. For Eurofer and F82H used in the blanket structure, the VV would take an excess of 250 years to satisfy LLW criteria, compared to over 500 years for G91. The uncertainty in ^{63}Ni-production in SS316 varied for each shielding material employed, translating to an uncertainty in time taken to reach the LLW limit of 0.3 years for Eurofer, 3.9 years for F82H and 5.5 years for G91. Not only would using G91 throughout the reactor blanket result in a much higher activity of SS316, but the corresponding time uncertainty is also higher, making G91 unfavourable in that regard. However, the intended 100 years to LLW will be exceeded significantly by the VV for each shielding material case, hence classification as ILW would come into effect either way, requiring different measures of disposal. Thus, the use of RAFM steels would not yield any valuable advantage regarding the activity of the VV, at least for the present modelling.

Table 8: Summary of the activity of SS316 in the VV 100 years after EOL for each in-vessel case and corresponding time taken to reach UK LLW levels, the uncertainty of the cross-section producing the dominant nuclide (^{63}Ni) and corresponding uncertainty in time to reach LLW.

Shielding Material	**VV Activity (Bq/kg)**	**Nuclide Production Cross-section**	**Uncertainty**	**Time to LLW (years)**	**Δt to LLW (years)**
Eurofer	8.05E+07	^{62}Ni(n,γ)^{63}Ni	0.21%	>250	0.3
F82H	8.03E+07	^{62}Ni(n,γ)^{63}Ni	2.76%	>250	3.9
G91	9.85E+07	^{62}Ni(n,γ)^{63}Ni	3.85%	>500	5.5

Since this study employed a very simplified, one-dimensional reactor model utilising homogenised material cells in the neutron transport calculations, the authors emphasise that the calculated activities, uncertainties and time-scales are subject to those simplifications. Uncertainties were calculated only for the production of radionuclides deemed "dominant"; other sources of uncertainty in the model or approach were not investigated in this study and should be addressed separately. Whereas this model is representative of a cross-section through the blanket and vacuum vessel, other parts of the reactor, such as the divertor, were not considered. Hence a more realistic reactor model may lead to different results including material activity and time-to-LLW. Since the feasibility of this method of combining activation calculations with nuclear data uncertainty propagation has now been demonstrated, a similar investigation may be carried out in the future with more mature reactor

models and nuclear data.

4. Conclusion

Neutron transport simulations and material inventory calculations were performed to obtain the activity of the RAFM steels Eurofer, F82H and the FM steel G91 for in-vessel use as well as for SS316 in the VV. Subsequently, a series of uncertainty analyses were conducted to investigate the effect of nuclear data uncertainties on the overall prediction of time required for activated materials to reach UK LLW limits after reactor end-of-life. Overall, it can be concluded from this study that:

- RAFM steels were activated significantly less than G91, but none of the assessed in-vessel steels met LLW activity levels in the FW and for large parts of the blanket far beyond 100 years. At the rear of the blanket (BSS), Eurofer, F82H and G91 all achieved LLW limits within 45 years of EOL. Even with the use of Eurofer or F82H, it will not be possible to decommission the entire blanket as LLW within 100 years of EOL.

- In the VV, the activity of SS316 was more than one order of magnitude above the LLW limit due to its high Ni-content. Therefore, the VV will not meet LLW requirements for centuries.

- The make-up of dominant nuclides in the FW varied with each material composition, whereas activity in the BSS was mainly caused by ^{55}Fe and ^{60}Co, due to neutron flux softening.

- The mean time-to-LLW for the FW exceeded 750 years for F82H and 1000 years for Eurofer and G91. In the outermost 5 cm of the blanket (BSS), this was approximately 36, 32 and 40 years for Eurofer, F82H and G91, respectively.

- Uncertainties in the production cross-sections of dominant nuclides were propagated to estimate error margins for the calculated time needed to reach the LLW limit. This resulted in a time uncertainty of no more than three years in the BSS and up to six years in the VV.

- Nuclear data uncertainties are only a small part of a large set of uncertainty contributors affecting quantities such as reactor lifetime, activity, dose levels as well as operational and decommissioning costs. However, the uncertainties found in the selected nuclear data alone were sufficient to potentially shift the point at which steels meet the UK LLW activity limit by several years.

- The feasibility of a rigorous methodology to perform independent uncertainty analyses on nuclear data has been demonstrated. The authors recommended

that similar analyses be carried out regularly in the future, when covariance matrix data become more mature in the available nuclear data libraries and parameters (material composition, irradiation scenario, etc.) are more refined. It is highlighted that this method is translatable to the modelling of other quantities or radiological predictions directly and indirectly related to radionuclide production. As existing literature on nuclear data uncertainties and their effects is scarce, further studies could generate valuable understanding relevant to the planning and implementation of nuclear fusion as an established energy source.

5. Acknowledgements

This work was partially carried out within the framework of the EUROfusion Consortium, funded by the European Union via the Euratom Research and Training Programme (Grant Agreement No 101052200 — EUROfusion) and from the EPSRC Energy Programme (grant number EP/W006839/1). Views and opinions expressed are however those of the authors only and do not necessarily reflect those of the European Union or the European Commission. Neither the European Union nor the European Commission can be held responsible for them.

Appendix A. Sample Appendix Section

Elemental compositions of the evaluated steels are summarised below in Table A.9.

Table A.9: Elemental compositions for Eurofer [27], F82H [28], G91 (T2) [8] and SS316 [2]

Element	**Composition (wt.%)**			
	Eurofer	**F82H**	**G91 (T2)**	**SS316L(N)-IG**
Fe	Base	Base	Base	Base
Al	0.01	0.01	0.02	-
Ag	-	0.002	-	-
As	0.05	0.002	0.01	-
B	0.002	0.0003	0.001	0.001
C	0.11	0.1	0.12	0.03
Co	0.01	0.005	-	0.05
Cr	9	8	9.5	18
Cu	0.01	0.01	0.1	0.3
Mn	0.4	0.1	0.5	2
Mo	0.005	0.001	1.05	2.7
N	0.03	0.005	0.07	0.08
Nb	0.005	0.00005	0.1	0.01
Ni	0.01	0.03	0.2	12.5
O	0.01	0.005	-	-
P	0.005	0.005	0.02	0.025
S	0.005	0.002	0.005	0.01
Sb	0.05	0.0005	0.03	-
Sn	0.05	0.001	0.01	-
Si	0.05	0.1	0.4	0.5
Ta	0.12	0.04	-	0.01
Ti	0.02	0.05	0.01	0.1
V	0.2	0.2	0.25	-
W	1.1	2	0.05	-
Zr	0.05	-	0.01	-

References

[1] M. Hernández-Mayoral, M. Caturla, 8 - microstructure evolution of irradiated structural materials in nuclear power plants, Woodhead Publishing (2010) 189–235doi:https://doi.org/10.1533/9781845699956.2.189.
URL `https://www.sciencedirect.com/science/article/pii/B9781845695118500081`

[2] M. Gilbert, T. Eade, C. Bachmann, U. Fischer, N. Taylor, Activation, decay heat, and waste classification studies of the European DEMO concept, Nuclear

Fusion 57 (4) (2017) 046015. doi:10.1088/1741-4326/aa5bd7.
URL https://iopscience.iop.org/article/10.1088/1741-4326/aa5bd7

[3] M. Gilbert, T. Eade, T. Rey, R. Vale, C. Bachmann, U. Fischer, N. Taylor, Waste implications from minor impurities in European DEMO materials, Nuclear Fusion 59 (7) (2019) 076015. doi:10.1088/1741-4326/ab154e.
URL https://iopscience.iop.org/article/10.1088/1741-4326/ab154e

[4] R. Pampin, S. Zheng, S. Lilley, B. Na, M. Loughlin, N. Taylor, Activation analyses updating the ITER radioactive waste assessment, Fusion Engineering and Design 87 (7-8) (2012) 1230–1234. doi:10.1016/j.fusengdes.2012.02.110.
URL https://linkinghub.elsevier.com/retrieve/pii/S0920379612001846

[5] B. van der Schaaf, F. Tavassoli, C. Fazio, E. Rigal, E. Diegele, R. Lindau, G. LeMarois, The development of eurofer reduced activation steel, Fusion Engineering and Design 69 (1) (2003) 197–203, 22nd Symposium on Fusion Technology. doi:https://doi.org/10.1016/S0920-3796(03)00337-5.
URL https://www.sciencedirect.com/science/article/pii/S0920379603003375

[6] H. Tanigawa, E. Gaganidze, T. Hirose, M. Ando, S. Zinkle, R. Lindau, E. Diegele, Development of benchmark reduced activation ferritic/martensitic steels for fusion energy applications, Nuclear Fusion 57 (9) (2017) 092004. doi:10.1088/1741-4326/57/9/092004.
URL https://iopscience.iop.org/article/10.1088/1741-4326/57/9/092004

[7] A.-A. Tavassoli, A. Alamo, L. Bedel, L. Forest, J.-M. Gentzbittel, J.-W. Rensman, E. Diegele, R. Lindau, M. Schirra, R. Schmitt, H. Schneider, C. Petersen, A.-M. Lancha, P. Fernandez, G. Filacchioni, M. Maday, K. Mergia, N. Boukos, Baluc, P. Spätig, E. Alves, E. Lucon, Materials design data for reduced activation martensitic steel type EUROFER, Journal of Nuclear Materials 329-333 (2004) 257–262. doi:10.1016/j.jnucmat.2004.04.020.
URL https://linkinghub.elsevier.com/retrieve/pii/S0022311504001485

[8] G. Bailey, O. Vilkhivskaya, M. Gilbert, Waste expectations of fusion steels under current waste repository criteria, Nuclear Fusion 61 (3) (2021) 036010. doi:10.1088/1741-4326/abc933.
URL https://doi.org/10.1088/1741-4326/abc933

[9] M. Fabbri, D. Leichtle, A. Martin, R. Pampin, E. Polunovskiy, Nuclear heat analysis for the iter vacuum vessel regular sector, Fusion Engineering and Design 137 (2018) 435–439. doi:https://doi.org/10.1016/j.fusengdes.2018.04.022.
URL https://www.sciencedirect.com/science/article/pii/S0920379618303107

[10] G. Stankunas, S. Breidokaite, A. Tidikas, Activation analysis and evaluation of radionuclide inventory decay heat for eu demo vacuum vessel components, Fusion Science and Technology 77 (7-8) (2021) 791–801. arXiv:https://doi.org/10.1080/15361055.2021.1906153, doi:10.1080/15361055.2021.1906153.
URL https://doi.org/10.1080/15361055.2021.1906153

[11] H. L. SWAMI, C. DANANI, A. K. SHAW, Activation characteristics of candidate structural materials for a near-term indian fusion reactor and the impact of their impurities on design considerations, Plasma Science and Technology 20 (6) (2018) 065602. doi:10.1088/2058-6272/aaabb4.
URL https://doi.org/10.1088/2058-6272/aaabb4

[12] P. Pereslavtsev, F. Cismondi, F. A. Hernández, Analyses of the shielding options for HCPB DEMO blanket, Fusion Engineering and Design 156 (2020) 111605. doi:10.1016/j.fusengdes.2020.111605.
URL https://linkinghub.elsevier.com/retrieve/pii/S0920379620301538

[13] M. R. Gilbert, T. Eade, C. Bachmann, U. Fischer, N. P. Taylor, Waste assessment of european DEMO fusion reactor designs, Fus. Eng. Des. 136 (2018) 42–48, special Issue: Proceedings of the 13th International Symposium on Fusion Nuclear Technology (ISFNT-13), https://doi.org/10.1016/j.fusengdes.2017.12.019.

[14] P. K. Romano, B. Forget, The openmc monte carlo particle transport code, Annals of Nuclear Energy 51 (2013) 274–281. doi:https://doi.org/10.1016/j.anucene.2012.06.040.
URL https://www.sciencedirect.com/science/article/pii/S0306454912003283

[15] D. Carloni, L. Boccaccini, F. Franza, S. Kecskes, Requirements for helium cooled pebble bed blanket and r&d activities, Fusion Engineering and Design 89 (7) (2014) 1341–1345, proceedings of the 11th International Symposium on Fusion Nuclear Technology-11 (ISFNT-11) Barcelona, Spain, 15-20 September, 2013. doi:https://doi.org/10.1016/j.fusengdes.2014.02.036.
URL https://www.sciencedirect.com/science/article/pii/S0920379614001203

[16] J.-C. Sublet, J. Eastwood, J. Morgan, M. Gilbert, M. Fleming, W. Arter, Fispact-ii: An advanced simulation system for activation, transmutation and material modelling, Nuclear Data Sheets 139 (2017) 77–137, special Issue on Nuclear Reaction Data. doi:https://doi.org/10.1016/j.nds.2017.01.002.
URL https://www.sciencedirect.com/science/article/pii/S0090375217300029

[17] I. Kodeli, S. Slavič, SUSD3D computer code as part of the XSUN-2017 windows interface environment for deterministic radiation transport and cross-section

sensitivity-uncertainty analysis, Science and Technology of Nuclear Installations 2017 (2017) 1–16. doi:10.1155/2017/1264736.

[18] R. E. MacFarlane, TRANSX 2: A code for interfacing MATXS cross-section libraries to nuclear transport codes (7 1992).
URL https://www.osti.gov/biblio/5133321

[19] PSR-0317 TRANSX-2.15 nuclear energy agency, https://www.oecd-nea.org/tools/abstract/detail/psr-0317/04, version: 05/01/2018.

[20] R. E. Alcouffe, R. S. Baker, J. A. Dahl, S. A. Turner, R. C. Ward, Partisn 5.97, 1-d, 2-d, 3-d time-dependent, multi- group deterministic parallel neutral particle transport code, la-ur-08-07258, NEA/Data Bank CCC-0760/01 Computer Code Collection (11 2008).
URL https://www.oecd-nea.org/tools/abstract/detail/ccc-0760/

[21] CCC-0760 PARTISN 5.97 nuclear energy agency, https://www.oecd-nea.org/tools/abstract/detail/ccc-0760/01, version: 02/11/2009.

[22] I. Kodeli, Multidimensional deterministic nuclear data sensitivity and uncertainty code system, method and application, Nuclear Science and Engineering 138 (2001) 45–66.

[23] NEA-1628 SUSD3D nuclear energy agency, https://www.oecd-nea.org/tools/abstract/detail/nea-1628/03, version: 2008.

[24] A. J. Koning, D. Rochman, TENDL-2017, release Date: April 25, 2018. Available from https://tendl.web.psi.ch/tendl_2017/tendl2017.html (2017).

[25] The JEFF team, JEFF-3.3: Evaluated nuclear data library, release Date: November, 20 (2017).
URL https://www.oecd-nea.org/dbdata/jeff/jeff33/index.html

[26] C. Liu, H. Yang, J. Zhang, J. Zhang, L. Li, Y. Qiu, D. Yao, X. Gao, Current status and progress on the shielding blanket of cfetr, IEEE Transactions on Plasma Science 46 (5) (2018) 1417–1421. doi:10.1109/TPS.2018.2792453.

[27] F. Tavassoli, Eurofer Steel, Development to Full Code Qualification, Procedia Engineering (2013) 9.

[28] L. Tan, Y. Katoh, A.-A. Tavassoli, J. Henry, M. Rieth, H. Sakasegawa, H. Tanigawa, Q. Huang, Recent status and improvement of reduced-activation

ferritic-martensitic steels for high-temperature service, Journal of Nuclear Materials 479 (2016) 515–523. doi:https://doi.org/10.1016/j.jnucmat.2016.07.054. URL https://www.sciencedirect.com/science/article/pii/S0022311516304755